16th European Signal Processing Conference (EUSIPCO 2008), Lausanne, Switzerland, August 25-29, 2008, copyright by EURASIP

MR ARTIFACT REDUCTION IN THE SIMULTANEOUS ACQUISITION OF EEG AND FMRI OF EPILEPTIC PATIENTS

L. Amini[1,2], *R. Sameni*[1,3], *C. Jutten*[1], *G.A. Hossein-Zadeh*[2], *H. Soltanian-Zadeh*[2,4]

[1]GIPSA-LAB, INPG, 46 Avenue Félix Viallet,38031,Grenoble cedex, France
[2]Control and Intelligent Processing Center of Excellence, Electrical and Computer Engineering Department, College of Engineering, University of Tehran, Tehran, Iran
[3]School of Electrical Engineering, Sharif University of Technology, Tehran, Iran
[4]Radiology Image Analysis Laboratory, Henry Ford Hospital, Detroit, MI 48202 USA
Emails: {ladan.amini, reza.sameni, christian.jutten}@gipsa-lab.inpg.fr; ghzadeh@ut.ac.ir, hamids@rad.hfh.edu

ABSTRACT

Integrating high spatial resolution of functional magnetic resonance imaging (fMRI) and high temporal resolution of electroencephalogram (EEG) is promising in simultaneous EEG and fMRI analysis, especially for epileptic patients. The EEG recorded inside an MR scanner is interfered with MR artifacts. In this article, we propose new artifact reduction approaches and compare them with the conventional artifact reduction methods. Our proposed approaches are based on generalized eigenvalue decomposition (GEVD) and median filtering. The proposed methods are applied on experimental simultaneous EEG and fMRI recordings of an epileptic patient. The results show significant improvement over conventional MR artifact reduction methods.

1. INTRODUCTION

Although simultaneous acquisition of EEG and fMRI may be essential for exploring the dynamics and localization of neural activity, several artifacts interfere the resulting EEG. These artifacts include: 1) MR artifacts, 2) RF pulse artifacts, and 3) Balistocardiogram (BCG) artifacts. The MR artifact is caused by the switching of the magnetic filed gradients used in the image acquisition, which induces unwanted voltages on the EEG recordings. The RF pulse artifact is due to the time varying electromagnetic field pulses (RF pulses) used for excitation in MRI recordings [1]. Although, the RF pulse has a very high frequency (in the order of 10 to 100 megahertz); but it is nonlinearly rectified to low frequencies (below 100Hz), within the EEG bandwidth. BCG artifact is caused by the micro motions of head EEG leads and wires within the static magnetic field. These motions are related to the pulsatile blood-flow in the head.

Different methods have been proposed for removing MR artifacts. Sparse component decomposition on the wavelet and discrete cosine basis [2], blind source extraction (BSE) followed by averaging-and-subtraction [3], and adaptive finite impulse response (FIR) filtering [4], are among these methods. Grouiller *et al.* [5] have compared some common methods such as image artifact reduction (IAR) [6], independent component analysis (ICA), fMRI artifact slice template removal (FASTR) [7], and filtering in the frequency domain using the Fourier transform on simulated and real data. IAR [6] is a conventional method based on subtraction of the averaging artifact waveform followed by adaptive noise cancellation (ANC). FASTR is the combination of principal component analysis (PCA) and IAR. Among the compared methods of [5], IAR was shown to be the most effective method. This method is widely used for MR artifact removal in the literature.

In this article, we propose new approaches for MR artifact reduction. The proposed methods are based on generalized eigenvalue decomposition (GEVD) [8], [9], [10], [11], and median filtering. In fact, EEG signals having MR artifacts have both stationary and non-stationary properties at different time scales. MR artifacts include temporal structures that can be considered stationary. On the other hand, due to the switching of the magnetic field gradient, EEG contaminated with MR artifact is non-stationary in the time domain. In this work, two representations of MR artifact using this prior information have been utilized in an iterative GEVD scheme, together with a median and low-pass filter to extract the MR artifact. The results of the proposed method are compared with the IAR method over real simultaneous EEG and fMRI of epileptic patients.

The organization of the paper is as follows. Section 2, explains the GEVD and its application in source separation. The proposed MR artifact reduction approaches are presented in Section 3. Section 4 is devoted to the experimental results by reporting the results and quantitative comparison of the conventional IAR method and the proposed methods. Concluding remarks are presented in Section 5.

2. REVIEW OF GENERALIZED EIGENVALUE DECOMPOSITION

We assume zero-mean N-dimensional non-stationary observations $\mathbf{x}(t)$ that are mutually dependent in different N channels[1]. We are interested in linear mixtures of the form $y(t) = \mathbf{w}^T\mathbf{x}(t)$ that satisfy some measure of signal separability. For this, we define the following cost function:

$$J(\mathbf{w}) \doteq \frac{E_\theta\{y(\theta)y(\theta+\tau_\theta)\}}{E_t\{y^2(t)\}} \tag{1}$$

where $E_t\{\cdot\}$ represents averaging over t, and θ and τ_θ are respectively the time intervals and the time-varying lags that are found from our *a priori* knowledge of the signal's structure and non-stationarity. By maximizing this cost function, we are looking for the $y(t)$ with bounded energy and with a maximal lagged correlation over specific time intervals (θ) and time-lags (τ_θ).

[1]Such signals can for example be the output of a linear process of the form $\mathbf{x}(t) = A\mathbf{s}(t) + \mathbf{n}$ where $A \in \mathbb{R}^{N\times M}$

Equation (1) can be rewritten as follows:

$$J(\mathbf{w}) = \frac{\mathbf{w}^T B_x \mathbf{w}}{\mathbf{w}^T C_x \mathbf{w}} \tag{2}$$

where

$$C_x \doteq E_t\{\mathbf{x}(t)\mathbf{x}(t)^T\} \tag{3}$$

and

$$B_x \doteq E_\theta\{\mathbf{x}(\theta)\mathbf{x}(\theta+\tau_\theta)^T\} \tag{4}$$

The matrix C_x is the covariance matrix of $\mathbf{x}(t)$, which is known to be symmetric and positive definite. On the other hand, the matrix B_x is not generally symmetric and we need to make it symmetric ($B_x \leftarrow (B_x + B_x^T)/2$) for further use [2].

Equation (2) is in the form of the *Rayleight quotient* [11], and its maximum value is achieved through the joint diagonalization of the matrix pair (B_x, C_x):

$$\begin{cases} W^T B_x W = \Lambda \\ W^T C_x W = I \end{cases} \tag{5}$$

where Λ is a diagonal matrix containing real generalized eigenvalues on its diagonal (in descending order), and $W = [\mathbf{w}_1, ...\mathbf{w}_N]$ is the matrix containing the corresponding generalized eigenvectors as its columns. The input signals may next be decomposed as follows:

$$\mathbf{y}(t) = W^T \mathbf{x}(t) \tag{6}$$

where $\mathbf{y}(t) = [y_1(t), ..., y_N(t)]^T$ has decorrelated components, with the first component maximizing defined quotient in (2).

3. PROPOSED MR ARTIFACT REDUCTION APPROACHES

In Fig.1, a typical segment of EEG contaminated with MR artifacts of two channels is depicted. MR artifacts are MR scanner dependent. MR artifact of the MR scanner used for our data are repeated with a period of three seconds, with two seconds of activation in each period (while magnetic field gradient was on). A closer look at the MR artifacts of each period, shows sharp regular peaks with dominant high amplitudes that are repeated every 62-63 samples (indicated with circles in Fig.1). Each peak is also surrounded by several smaller peaks.

In the previous section, we noticed that the components extracted by GEVD are ranked according to an order that depends on the statistics carried by the matrix B_x. The spatial whiteness of the extracted components is guaranteed by the diagonalization of C_x. Here, our objective is to use the above mentioned properties of the MR artifact structure to form the matrix B_x, such that it contains the statistical properties of these artifacts. Therefore, since the $y_i(t)$ calculated from (6) are sorted in descending order of their corresponding eigenvalues, the MR artifacts are expected to be most concentrated in the first few components. In the following, two models of MR artifact (B_x) using this prior information are presented.

a. *First Statistical Measure*

In the first approach, we first detect the dominant MR peaks from an arbitrary channel. Due to the stationarity of these peaks, a robust method for detecting the peaks is a *matched filter* that uses a typical MR artifact segment as its template filter. A window is considered around each sharp peak of MR artifact. The resulted windowed segment is assumed to be stationary. Hence the average of the correlation matrices of windowed segments of two proceeding peaks can be a good model of statistical properties of MR artifact. In other words since the MR artifacts of different channels are rather regular, the samples that are equally distanced from each peak are highly correlated with one another. We can therefore, calculate the correlation between the windows surrounding each peak as a statistical property of the MR artifacts. Carrying out this procedure over the different channels, i.e., by considering each time sample of the different channels as an N-dimensional vector, we can redefine the matrix B_x defined in (4) as follows:

$$B_{x1} = E_\theta\{\mathbf{x}(\theta)\mathbf{x}(\theta+\Delta p_i)^T\} \tag{7}$$

where $\Delta p_i = p_{i+1} - p_i$ and $\theta \in \{\text{MR artifact time interval}\}$. p_i is the location of the i-th sharp peak of the MR artifact in the original data.

b. *Second Statistical Measure*

In the first model, the covariance matrix B_{x1} was calculated by direct vector-by-vector multiplication of the samples of short windows of $\mathbf{x}(\theta)$. According to Fig. 1, each of these windows, consists of a high-amplitude MR artifact peak and a few smaller peaks around it. Therefore, in the statistical measure B_{x1}, each sample will have a contribution as strong as its energy. In other words, the smaller peaks around the dominant peaks of MR artifacts will have less influence on the statistics of B_{x1} and the GEVD procedure will make less effort to remove such peaks from the input signal. However, the strong and weak MR artifacts are somehow equally destructive in EEG analysis. We can therefore attempt in equalizing the peaks before the calculation of our statistical measure. This idea leads us to the following definition of the MR artifact covariance matrix:

$$B_{x2} = E_\theta\{[\mathbf{F}(\theta) \otimes \mathbf{x}(\theta)][\mathbf{F}(\theta) \otimes \mathbf{x}(\theta)]^T\} \tag{8}$$

where the operator $\otimes$ represents sample-by-sample multiplication, and $\theta \in \{\text{MR artifact time interval}\}$. $\mathbf{F}(\theta)$ is a column of the matrix including weighting function in each row. The *ad hoc* weighting function equalizes the peak amplitudes

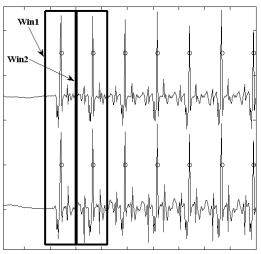

Figure 1: Peak detection and windowing on MR artifact of EEG signal. Peaks are shown with circles.

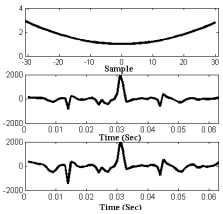

Figure 2: Weighting effect on windowed segments. From top to bottom, the window function, a typical windowed segment before and after weighting.

[2] Note that here we are not concerned by the non-positive definiteness of B_x; since it is verified experimentally that most of the eigenvalues have positive values and negative eigenvalues have significantly smaller absolute values than the positive ones.

of the windowed segments. Fig. 2 shows from top to bottom one row of $\mathbf{F}(\theta)$, a typical windowed segment and the corresponding weighted windowed segment, respectively. B_{x2} is the average of weighted windowed segments energies.

3.1 Nonlinear Median Filtering

The GEVD procedure provides a means of transforming the input data, into components that are ranked according to their similarity with the MR artifacts. However, due to the linearity of the transformation (6), the performance of this primary stage is limited and it can not fully separate the MR artifacts from other components (including the EEG) except if the contaminated EEG signal perfectly satisfies a linear mixture ($\mathbf{x} = A\mathbf{s} + \mathbf{n}$), with a moderately low noise and a sufficient number of observation channels. Here the model of contaminated EEG signal is rather complex as proved by our obtained results of applying linear ICA. Here we propose the GEVD followed by a nonlinear denoising procedure that is applied to the first D ($D < N$) components of the GEVD outputs while keeping the rest of $(N-D)$ components unchanged. This nonlinear denoising may indeed be applied to the original channels too (without the GEVD procedure) that is our third proposed approach (Fig. 3.c); but in this case we would not benefit from the mutual information of the different channels. In fact, since the GEVD procedure concentrates the energy of the MR artifacts in the first few components, the EEG (non-MR artifact) components are less influenced by the nonlinear filtering when we apply this filter at the output of the GEVD procedure.

In this study, a two-step *moving window median* (MWM) filter was used for nonlinear filtering. A theoretical study of the MWM filter and its extensions may be found in [12]. The first median filter highly attenuates the sharp peaks, while the second one (with a wider window length) reduces the remaining peaks and smoothes the results. As a rule of thumb, the median filter window lengths should be wider than the width of the MR artifacts. Therefore, with proper choice of median filter width, peaks such as the MR artifacts are less likely to pass the MWM filter and by subtracting the output of the second MWM filter from the input signal, we can assure that the MR artifact peaks are effectively removed, while the EEG components are least influenced. The MWM filter is further followed by a low-pass filter, to suppress the possible out of band components introduced by the nonlinear MWM filter and higher frequencies that are not interested in EEG analysis. After applying the filtering procedure denoted above (Median-LPF) to the first D components of GEVD, the D filtered and $(N-D)$ unchanged components are back-projected to the input space using the inverse of the decomposing matrix W^T (Fig. 3.a). The preprocessed data, denoted by X in Fig. 3, is the matrix including preprocessed EEG channels in each row. Preprocessed data is contaminated EEG with MR artifact without dc and linear trend. To detrend, the best straight-line fit is removed from each processed channel segment.

3.2 Iterative Denoising

Up to this point, we have improved the input signal quality by applying GEVD (using either B_{x1} or B_{x2}), the nonlinear filtering procedure, and the back-projection. This procedure may be repeated in several iterations, each time over the output of the previous run. This leads to a deflation procedure that removes one (or more) dimensions of the MR artifacts in each iteration and is repeated until the residual signals are 'sufficiently clean'. For this, we need some measure of signal cleanness that can be used as the stopping criterion of the iterative procedure. Due to the switching magnetic field gradient, we propose to use the ratio between the signal energy of the MR artifact time intervals (θ) over the rest of data, i.e. when the magnetic field gradient is off ($\tilde{\theta}$)):

$$C = E_{ch}\{\frac{E_{\theta}\{\hat{x}_{ch}^2(\theta)\}}{E_{\tilde{\theta}}\{\hat{x}_{ch}^2(\tilde{\theta})\}}\} \tag{9}$$

where $\hat{x}(t)$ is the cleaned data of each channel in each iteration and $E_{ch}\{\cdot\}$ is averaging over channels. The iterative procedure is stopped when the normalized difference of cleaning criteria between two iterations is less than a predefined threshold.

We hereby refer to this algorithm as Iterative GEVD. The overall flowchart of this algorithm is depicted in Fig. 3.a. Following, the two statistical measures defined in (7) and (8), the iterative procedure can either be based on B_{x1}, which we call Iterative GEVD-Similarities (IGS), or on B_{x2}, which we call Iterative GEVD-Weighted (IGW). The flowcharts of IGS and IGW are depicted in Fig. 3.b.

4. EXPERIMENTAL RESULTS

4.1 Data

The recordings were made in the 3T scanner (3T Bruker BioSpin, Bruker Medizintechnik GmbH, Ettlingen, Germany) utilizing an MR compatible EEG amplifier (SD32, Micromed, Treviso, Italy) with 17 c-shaped electrodes positioned according to the 10/20 system (O1 and O2 were not used for subjects comfort). The reference electrode was at Oz. A Gradient-Echo Echo Planar Imaging (GE-EPI) sequence used for MR image acquisition [5]. The sampling rate of EEG acquisition was 1024Hz. An anti-aliasing hardware low-pass filter with cut-off frequency of 286.8Hz was applied. EEG signals were calibrated with a square wave of 100μV utilizing an external calibrator plugged on all inputs. The epileptic patient was required to keep eyes closed and relax during the experiment.

4.2 Results

Initially, the data were preprocessed for DC and trend removal. The three proposed approaches were applied on the

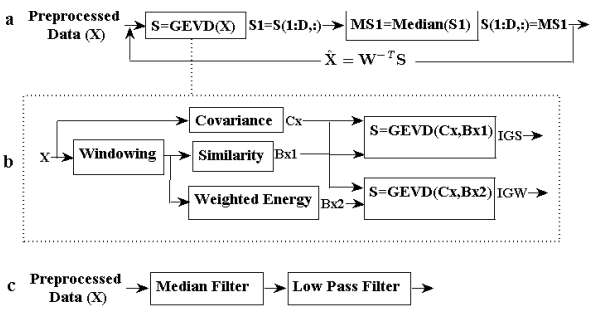

Figure 3: Flowchart of proposed MR artifact reduction algorithms. (a) Iterative GEVD; (b) IGS and IGW, and (c) Median-low-pass filtering. D is the number of first few components in which the MR artifact is most amplified.

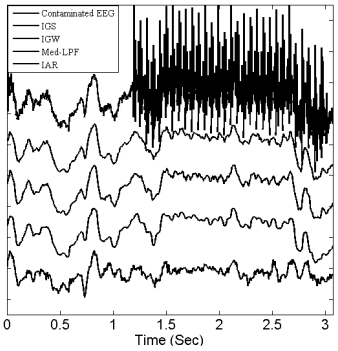

Figure 4: Comparison of methods in reducing MR artifact from EEG signal. From up to bottom, contaminated EEG signal with MR artifact, the processed signal by IGS, IGW, Med-LPF, and IAR.

preprocessed data. For the first two approaches (IGS and IGW), as explained before, the sharp peaks of the MR artifacts were detected using a matched filter (Fig. 1). Next, C_x, B_{x1} and B_{x2} were calculated according to the procedures explained in previous sections. In the IGS method B_{x1} and C_x were jointly diagonalized, while in the IGW approach B_{x2} and C_x were jointly diagonalized. In each iteration of the proposed procedure, the first $D = 3$ of the $N = 15$ components extracted by GEVD, were denoised by the nonlinear MWM filter. The choice of D was based on empirical study of the output of the GEVD stage; the final results are not very sensitive to the value of $D > 3$. In the nonlinear filtering step, the first and second MWM window lengths used in the denoising were 20 and 40 samples (about 20ms and 40ms), respectively, since the typical width of sharp MR artifact peaks are about 20ms. The low-pass filter following the MWM filter was a first-order filter with a cut-off frequency of 45Hz, which is close to the effective bandwidth of the EEG. Next, the filtered and unchanged components were back-projected using the inverse of the decomposing matrix. This procedure was repeated until the normalized difference of the cleaning criteria defined in (9) between two consecutive iterations became less than 0.001. This limit was typically reached around 16 iterations. In Fig. 4, a typical segment of contaminated EEG and the results of IGS and IGW are shown. For comparison, the results of the Median-LPF and IAR [6, 5] are added in Fig. 4.

4.3 Evaluation Methods

Fig. 4, compares the proposed methods with the IAR method presented in [6, 5]. It is necessary to define an objective criterion for comparing the methods quantitatively. Since there is no ground truth, measuring the performance of each method is challenging. A first idea is to compare the signal with a reference which could be the signal acquired out of scanner or the time segment without MR artifact. The EEG signal inside and outside of MR scanner of a patient even with the same electrode locations are not necessarily similar. The EEG itself is very non-stationary in the time domain, especially for epileptic patients, since the IEDs (Interictal Epileptiform Discharges) appear spontaneously and the shape of IEDs are different. Due to this problem, the EEG contaminated with MR artifact and cleaned signal were compared. Comparable methods in the time domain were

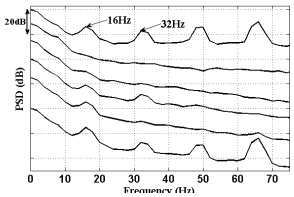

Figure 5: Comparison of the PSDs. From up to bottom, PSD of contaminated EEG signal, outer scanner EEG signal, and the processed signal by IGS, IGW, Med-LPF, and IAR.

evaluated. The cleaned data were segmented around each peak of the MR artifact. The similarity between each two proceeding segments or all the segments was calculated. In other words, the periodicity of the cleaned data around each peak was measured. The cleaned data preserves the periodicity under each peak if the artifact removal method has not reduced MR artifact perfectly. In another method, the similarity between cleaned and original data under each sharp peak was measured. The cleaned data has some overshoots under each peak when the artifact removal method has not worked efficiently. However, since these methods of evaluation were not consistent for different MR artifact removal approaches, we compared spectral indexes of the EEG that are known to be more consistent. The following three criteria were defined for this purpose:

$$\begin{aligned} F_1 &= 10log_{10}E_{ch}\{\tfrac{E_i\{\hat{P}(fp_i)\}}{E_i\{P(fp_i)\}}\} \\ F_2 &= 10log_{10}E_{ch}\{E_i\{\tfrac{\hat{P}(fp_i)}{P(fp_i)}\}\} \\ F_3 &= 10log_{10}E_{ch}\{\tfrac{E_{i=17,34}\{\hat{P}(fp_i)\}}{E_{i=17,34}\{P(fp_i)\}}\} \end{aligned} \tag{10}$$

where $E_{ch}\{\cdot\}$ and $E_i\{\cdot\}$ are averages over channels and original data PSD peaks, respectively. P and $\hat{P}$ are the power spectral density (PSD) of the original and cleaned data, respectively. fp_i is an interval of 4Hz around the peak of the original data PSD in frequencies higher than 14Hz. This range is chosen since the interested spikes or IEDs appear below 14Hz. Since the sampling rate is not a multiple of the MR artifact frequencies, the energy of MR artifact frequencies can be distributed among a few frequency bins of the PSD. Therefore, an interval of 4Hz is considered around each PSD peak.

F_1 and F_2 calculate the PSD attenuation (in dB) of cleaned data around each peak of the original data PSD (first row of Fig. 5). The method that most attenuates the PSD peaks of the MR artifact is preferred. Since sharp peaks are repeated in MR artifact every 62 or 63 samples and the sampling rate is 1024Hz, peaks around 16-17 Hz and their harmonics in the PSD of the original data is related to MR artifact. Therefore, F_3 measures the attenuation around peaks of 16Hz and 32Hz that are shown in Fig. 5. The peaks in higher harmonics are not considered in F_3, because frequencies higher than 45Hz are not of interest in EEG analysis. PSD of contaminated EEG, EEG signal out of MR scanner, and the processed signal by IGS, IGW, Median-LPF, and IAR are depicted respectively from up to bottom in Fig. 5. To compute the PSD, the Discrete Fourier Transforms (DFT) of 0.5s windowed segments are calculated. To compare the results in high frequency resolution, the same criteria (F_1, F_2, and F_3) have been utilized, but the PSD is computed by the

Table 1: Frequency domain evaluation results (in dB) at low and high frequency resolutions. Orig-Out, IGS, IGW, Med-LPF, and IAR stand for original signal outside the MR scanner, Iterative GEVD-similarities, Iterative GEVD-weighted, Median-low-pass filter and Image Artifact Reduction [5], [6]

Frequency	Low Resolution			High Resolution		
Method(dB)	F_1	F_2	F_3	F_1	F_2	F_3
Orig-Out	-34	-33	-23	-35	-30	-25
IGS	-28	-27	-16	-28	-24	-17
IGW	-27	-25	-14	-26	-23	-15
Med-LPF	-26	-25	-13	-25	-22	-14
IAR	-21	-23	-11	-20	-21	-12

DFT of 9s windowed segments. The window length is chosen 9s since the gradient is switched on every 3 seconds. To measure how the cleaned data is following this period, several periods (e.g., 3 periods) are needed.

F_1, F_2 and F_3 in low and high frequency resolutions were calculated for IAR and the three proposed methods. It is important to mention that the low-pass filter applied on the results of the proposed methods utilized on the results of IAR method before F_1-F_3 calculation for comparing all the methods equally. The calculations of F_1-F_3 were carried out over 50 different 30s EEG segments for an epileptic patient. The average of 50 calculations of F_1-F_3 are reported in Table 1. The method that better reduces the MR artifact has greater absolute values of F_1-F_3 that is a necessary condition but not sufficient. Since the outer original signal has no MR artifact (no PSD peaks after 14Hz), F_1-F_3 for the outer scanner signal has the maximum absolute values that is the minimum resemblance to contaminated EEG with MR artifact. Hence the F_1-F_3 of the outer signal shows the minimum value in each column of Table 1.

By comparing the results of Table 1, it can be noticed that the proposed methods have outperformed the conventional IAR method. Among, the proposed methods first IGS, second IGW and third Median-LPF have better reduced the MR artifacts (using the defined criteria). In the IGS method, components of GEVD are well amplified in the first few components. But in the IGW the MR methods, MR artifact is not extracted as good as the IGS method. The Median-LPF method is very simple, but it does not consider the information between channels. It also does not use the prior information as much as the first two methods. The PSD attenuation in MR artifact peaks of the IGS method is comparable with the EEG acquired outside of the scanner. This method has effectively mitigated MR artifacts from contaminated EEG.

5. CONCLUSION

In simultaneous EEG and fMRI recording, MR artifact reduction is an important issue and the development of an efficient artifact removal algorithm has significant effect on further processing. We proposed three artifact removal methods using two models of MR artifact. The performance of our proposed artifact removal methods was evaluated on real epileptic patient data and appeared to outperform the conventional IAR method. The IGS method has shown better performance in MR artifact reduction compared to the other proposed methods. It is important to mention that as MR artifacts are MR scanner dependent, our method has been customized to the MR scanner used for our data. The presented algorithms were based on a linear model. Convolutive models will be studied in the future work for this purpose.

6. ACKNOWLEDGMENTS

We gratefully acknowledge Olivier David and Frédéric Grouiller for acquiring the data and the assistance at the beginning of this study.

REFERENCES

[1] M. Negishi, B. I. Pinus, A. B. Pinus, and R. T. Constable, "Origin of the Radio Frequency Pulse Artifact in Simultaneous EEG-fMRI Recording: Rectification at the Carbon-Metal Interface," *IEEE Trans. Biomed. Eng.*, vol. 54, no. 9, pp. 1725–1727, September 2007.

[2] P. Xu, H. Chen, Z. Liu, and D. Yao, "A New Method Based on Sparse Component Decomposition to Remove MRI Artifacts in the Continuous EEG Recordings," in *Proc. of the 2005 IEEE Trans. Biomed. Eng. 27th Annu. Conf.*, Shanghai (China), September 1–4 2005, pp. 2006–2008.

[3] M. Jing and S. Sanei, "Scanner Artifact Removal in Simultaneous EEG-fMRI for Epileptic Seizure Prediction," in *The 18th Int. Conf. on Pattern Recognition (ICPR'06)*, 2006, pp. 722–725.

[4] X. Wan, K. Iwata, J. Riera, M. Kitamura, and R. Kawashima, "Artifact Reduction for Simultaneous EEG-fMRI Recording- Adaptive FIR Reduction of Imaging Artifacts," *Elsevier, Clinical Neurophysiology*, vol. 117, pp. 681–692, 2006.

[5] F. Grouiller, L. Vercueil, A. Krainik, C. Segebarth, P. Kahane, and O. David, "A Comparative Study of Different Artefact Removal Algorithms for EEG Signals Acquired During Functional MRI," *Neuroimage*, vol. 38, pp. 124–137, 2007.

[6] P. Allen, O. Josephs, and R. Turner, "A Method for Removing Imaging Artifact from Continuous EEG Recorded During Functional MRI," *Neuro-Image*, vol. 12, pp. 230–239, 2000.

[7] R. K. Niazy, C. F. Beckmann, G. Iannetti, J. Brady, and S. Smith, "Removal of fMRI environment artifacts from EEG data using optimal basis sets," *NeuroImage*, vol. 28, pp. 720–737, 2005.

[8] R. Sameni, C. Jutten, and M. B. Shamsollahi, "Multichannel Electrocardiogram Decomposition using Periodic Component Analysis," *"IEEE Trans. Biomed. Eng. "*, [to appear] 2008.

[9] L. Parra and P. Sajda, "Blind Source Separation via Generalized Eigenvalue Decomposition," *Journal of Machine Learning Research*, pp. 1261–1269, 2003.

[10] L. Tong, R.-W. Liu, V. Soon, and Y.-F. Huang, "Indeterminacy and Identifiability of Blind Identification," *IEEE Trans. Circuits Syst.*, no. 5, pp. 499–509, May 1991.

[11] G. Strang, *Linear Algebra and Its Applications*, 3rd ed. Brooks/Cole, 1988.

[12] G. R. Arce, *Nonlinear Signal Processing: A Statistical Approach*. New York: John Wiley & Sons Inc., 2004.